Thermally Controlled Morphologies in a Block Copolymer Supramolecule via Nonreversible Order−Order Transitions

ARTICLE *in* MACROMOLECULES · JULY 2013

Impact Factor: 5.8 · DOI: 10.1021/ma401033w

3 AUTHORS, INCLUDING:

Peter Bai
University of California, Berkeley
17 PUBLICATIONS **166** CITATIONS

Macromolecules

Article

pubs.acs.org/Macromolecules

Thermally Controlled Morphologies in a Block Copolymer Supramolecule via Nonreversible Order−Order Transitions

Peter Bai,[†,§] Myung Im Kim,[†,∥] and Ting Xu*[,†,‡,§]

[†]Department of Materials Science and Engineering, University of California, Berkeley, Berkeley, California 94720, United States

[‡]Department of Chemistry, University of California, Berkeley, Berkeley, California 94720, United States

[§]Materials Sciences Division, Lawrence-Berkeley National Laboratory, Berkeley, California 94720, United States

Supporting Information

ABSTRACT: Block copolymer (BCP)-based supramolecules represent a versatile platform to generate functional nanostructures without the need for complex synthesis. The noncovalent bonding between the BCP and small molecules further opens opportunities to access thermal responsive assemblies. A BCP supramolecule containing cholesteric liquid crystal (LC) small molecules is observed to undergo thermally induced, nonreversible order−order transitions (OOTs), resulting in several well-defined morphologies readily tunable by annealing temperature. The nonreversible OOTs highlight the importance of small molecule phase transitions and intermolecular interactions on the overall phase behavior of the supramolecule. The present system also provides a route to manipulate local nanostructures via heating.

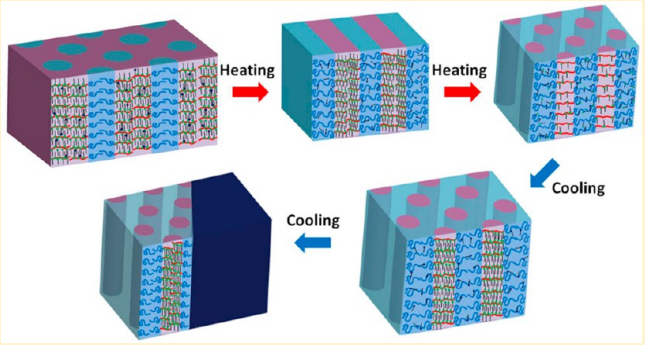

INTRODUCTION

Block copolymer (BCP)-based supramolecules, comprised of small molecules linked to BCP side chains via hydrogen bonding, electrostatic interactions, metal ligation, or $\pi-\pi$ interactions,[1−13] represent a facile way to incorporate functionalities and stimuli-responsiveness into the BCP system without complex synthesis.[14−21] Because of the noncovalent nature of the bond between BCP backbone and small molecule, the thermal phase behavior of the BCP supramolecule is more complex than that of BCP or small molecule. The thermal stability of noncovalent bond and intermolecular interactions between small molecules and each BCP block play critical roles in their phase behavior such as morphological transitions during thermal annealing.[22−25]

Extensive studies on the role of these intermolecular interactions have been carried out on supramolecules.[1,3,26−28] Multiple thermally reversible order−order transitions (OOTs) were routinely observed in supramolecules containing a weakly interacting alkylphenol as the side group. These OOTs were mainly due to the redistribution of small molecules upon thermal treatment, i.e., diffusion of small molecules out of the poly(4-vinylpyridine) (P4VP) microdomain during heating and reincorporation into P4VP during cooling process.[28] In contrast, in a supramolecule containing strongly interacting organic semiconductors, such as oligothiopenes, the assembly process follows a different kinetic pathway.[29] Oligothiopene molecules were first macrophase separated from the BCP due to their strong tendency to crystallize after solution casting. Upon heating, oligothiophene molecules get incorporated within the P4VP microdomain, leading to over 70% change in the BCP periodicity in the heating/cooling cycle.[30] Constructing supramolecules using liquid crystals can incorporate unique structural and optical properties. Their complex phase behavior and responsiveness to the external stimuli are also very attractive to manipulate supramolecular assemblies.[6,8,27,31,32] However, liquid crystals often have complex phase behavior as a function of temperature. There has been limited exploration in how the mobility and phase behavior of these complex molecules may change the kinetic pathway of the self-assembly process in a supramolecular system.

We investigated a family of BCP-based supramolecules containing a cholesteric small molecule. The supramolecule, called PS-*b*-P4VP(ChHP), comprised of polystyrene-*block*-poly(4-vinylpyridine) (PS-*b*-P4VP) and 3-hydroxylphenyl cholesteryl succinate (ChHP) hydrogen bonded to the 4VP units (Scheme 1), undergoes nonreversible OOT from a P4VP(ChHP) majority morphology to increasingly P4VP(ChHP) minority morphologies upon thermal annealing. The resulting morphology is readily tunable over several well-ordered structures by controlling the annealing temperature, allowing multiple morphologies to be obtained from a single starting material. The nonreversible OOTs are due to diffusion and subsequent macrophase separation of ChHP molecules out of the P4VP(ChHP) microdomain. The interface between the

Received: May 17, 2013
Revised: June 29, 2013
Published: July 12, 2013

Scheme 1. Formation of PS-*b*-P4VP(ChHP) Supramolecule via Hydrogen Bonding of ChHP Small Molecule to 4VP Units

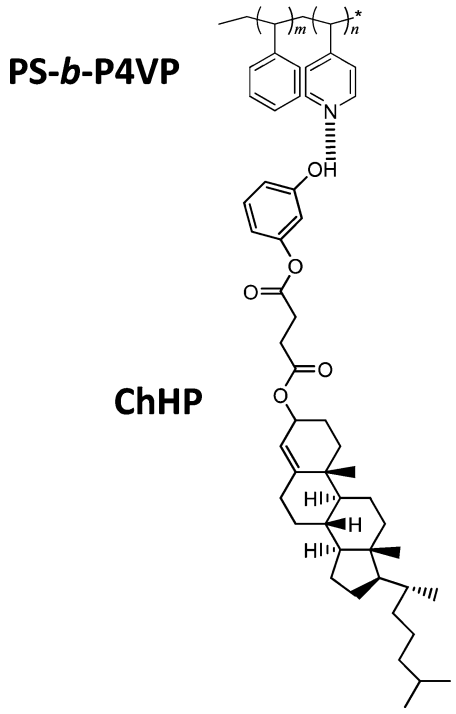

PS-*b*-P4VP(ChHP) and ChHP phases has very sharp ChHP concentration gradient, which ensures the homogeneity of the microphase-separated PS-*b*-P4VP(ChHP) morphology. The resulting nonreversible OOTs can be attributed to the miscibility between ChHP and each BCP block and the mobility and phase transitions of ChHP. This study provides useful insight into the role of molecular interactions and small molecule phase transitions on the thermal responsiveness and self-assembly kinetic pathway of BCP-based supramolecules. Since hydrogen-bonded small molecules can be selectively removed by an appropriate solvent,[33] the present study opens the opportunity to achieve local control of supramolecule morphology via local heating to generate heterogeneous morphologies.

EXPERIMENTAL SECTION

Materials. P4VP and PS-*b*-P4VP copolymers were purchased from Polymer Source, Inc. Chloroform was purchased from Fisher and used without any purification. The synthetic procedure of ChHP is described in detail in the Supporting Information (S1).

Supramolecule Sample Preparation. P4VP and PS-*b*-P4VP were first dissolved in chloroform to form 1–2% (w/v) stock solutions. The desired amount of ChHP was dissolved in chloroform. The PS-*b*-P4VP solution was then added dropwise to the ChHP solution, followed by stirring overnight. The resulting blend of PS-*b*-P4VP and ChHP was casted and dried in a Teflon beaker at room temperature in a chloroform atmosphere, allowing the solvent to slowly evaporate over 48 h. The blend was then annealed at 60 °C under vacuum for overnight to completely remove the solvent. The supramolecule samples are denoted as PS(m)-*b*-P4VP(n)$_1$(ChHP)$_1$, where m and n denote the molecular weight (in g/mol) of the PS and P4VP block, respectively; the molar ratio of 4VP:ChHP is maintained at 1 for all samples.

Fourier-Transform Infrared (FT-IR) Spectroscopy. Samples were cast between two NaCl pellets, and the absorption spectra were collected using a Nicolet 6700 FT-IR spectrometer. For *in situ* FT-IR, samples on NaCl pellets were heated from room temperature to 150

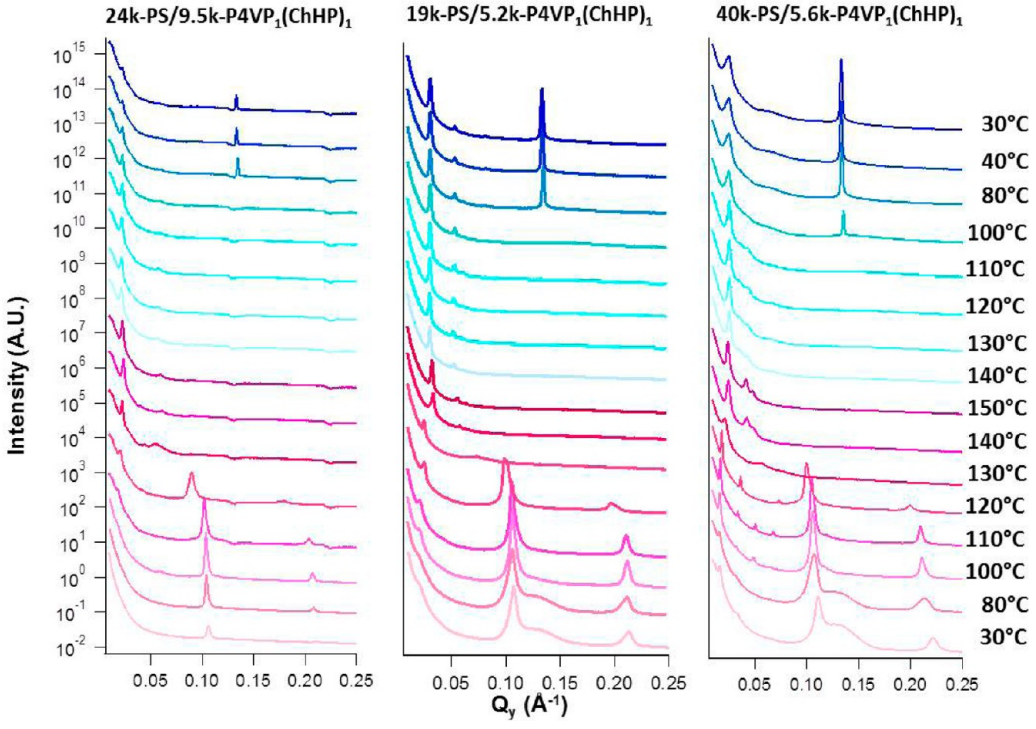

Figure 1. *In situ* SAXS plots of PS(24k)-*b*-P4VP(9.5k)$_1$(ChHP)$_1$ (left panel), PS(19k)-*b*-P4VP(5.2k)$_1$(ChHP)$_1$ (middle panel), and PS(40k)-*b*-P4VP(5.6k)$_1$(ChHP)$_1$ (right panel) supramolecules heated from 30 °C (bottom) to 150 °C and subsequently cooled back to 30 °C (top). All three supramolecules undergo a decrease in microdomain size upon heating, a small increase in microdomain size upon cooling, and a shift in the ChHP scattering peak to higher Q_y.

dx.doi.org/10.1021/ma401033w | *Macromolecules* 2013, 46, 5531–5537

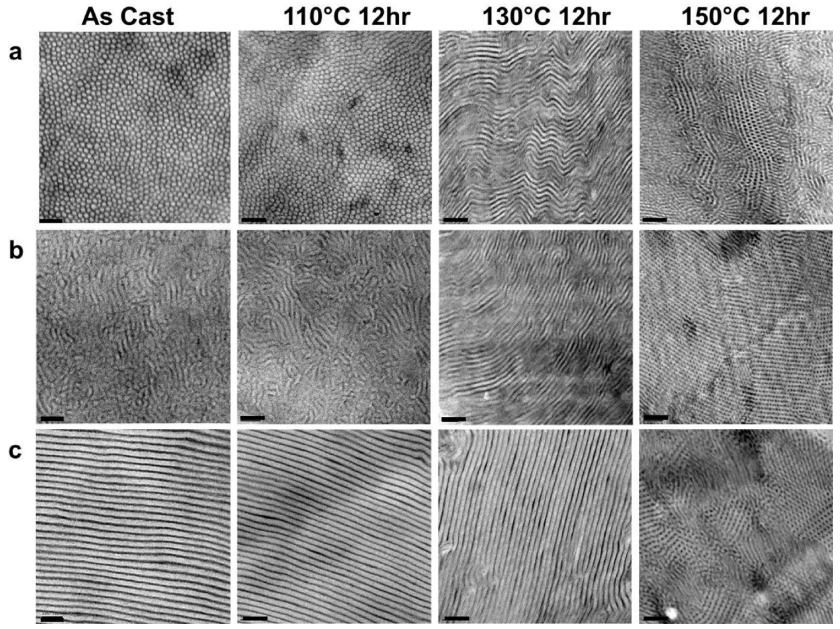

Figure 2. TEM images of (a) PS(24k)-*b*-P4VP(9.5k)$_1$(ChHP)$_1$, (b) PS(19k)-*b*-P4VP(5.2k)$_1$(ChHP)$_1$, and (c) PS(40k)-*b*-P4VP(5.6k)$_1$(ChHP)$_1$ in their as cast state and after thermal annealing at 110, 130, and 150 °C in vacuum for 12 h. The samples are stained with I_2 to enhance the contrast between PS (bright) and P4VP(ChHP) (dark) microdomains. Transitions from a P4VP(ChHP) comb block (dark) majority microphase to a comb block minority microphase are clearly seen in all three supramolecules. Scale bars are 100 nm for all images.

°C at a heating rate of 20 °C/min under nitrogen gas. Each spectrum was collected 10 min after reaching the targeted temperature.

Differential Scanning Calorimetry (DSC). Differential scanning calorimetry measurements were performed on a TA Instruments DSC Q200. The samples (~2 mg) were heated from 0 to 200 °C at a heating rate of 10 °C/min under nitrogen gas. Three heating and cooling cycles are performed to eliminate the thermal history of the samples. The transitions of ChHP were collected from the third heating and cooling cycle.

Polarized Optical Microscope (POM). Birefringence in the supramolecule samples was observed using Olympus BX 51 with crossed polarizers in reflection mode. Samples were cast from chloroform solution onto a silicon wafer and covered with a cover glass. Samples were put on the heating stage (Linkam TP 94) with a Linkam LTS 350 temperature controller. Samples were heated from room temperature to 150 °C at heating rate of 30 °C/min under nitrogen gas and cooled from 150 °C to room temperature at a cooling rate of 6 °C/min. Each image was taken 5 min after reaching the targeted temperature.

Small-Angle X-ray Scattering (SAXS). SAXS studies were carried out at the Advanced Light Source beamline 7.3.3. X-rays with a wavelength of 1.240 Å (10 keV) were used. Spectra were collected on an ADSC Quantum 4u CCD detector with an area of 188 mm × 188 mm (2304 pixels × 2304 pixels) or a Pilatus 1 M detector with an area of 169 mm × 179 mm (981 pixels × 1043 pixels). The 1D SAXS profiles were obtained by circularly averaging the 2D data. Prior to SAXS experiment, samples were mounted in standard differential scanning calorimetry pans, which were used as a heating stage during scanning. All SAXS profiles were measured after keeping the samples at each temperature for 10 min.

Transmission Electron Microscopy (TEM). For TEM observations, samples mounted in the DSC pan were annealed at 110, 130 and 150 °C for 12 h under vacuum and then slowly cooled to room temperature. Samples were embedded in resin (Araldite 502, Electron Microscopy Sciences) and cured at 60 °C overnight. Thin sections about 50 nm in thickness were microtomed using an RMC MT-X Ultramicrotome (Boeckler Instruments) and picked up on carbon-coated Cu grids on top of water. The thin sections were exposed to iodine vapor for 1 h to stain the P4VP domain selectively and imaged using a FEI Tecnai 12 TEM operating at 120 kV accelerating voltage or a JEOL 2100 TEM operating at 200 kV.

■ RESULTS AND DISCUSSION

Detailed information regarding synthesis of ChHP and supramolecule sample preparation is provided in the Supporting Information (S1). Briefly, the supramolecule samples are prepared by separately dissolving the BCP and ChHP in chloroform, mixing the two solutions to allow for hydrogen bonding formation, and drying the mixture. The supramolecule samples are denoted as PS(m)-*b*-P4VP(n)$_1$(ChHP)$_1$, where m and n denote the molecular weight (in g/mol) of the PS and P4VP block, respectively; the molar ratio of 4VP:ChHP is maintained at 1 for all samples.

The thermal phase behavior of the supramolecule is probed by *in situ* SAXS during heating from room temperature to 150 °C at a heating rate of 20 °C/min and subsequently cooling back to 30 °C (Figure 1, left panel). For PS(24k)-*b*-P4VP(9.5k)$_1$(ChHP)$_1$ at 110 °C, the SAXS profile has a scattering peak at q = 0.017 Å^{-1}, corresponding to a periodicity of 37 nm, characteristic of BCP microdomain size. In addition, there is a peak at q = 0.104 Å^{-1} and a second order peak at q = 0.208 Å^{-1}, corresponding to a lamellar structure with a periodicity of 6.18 nm. This is slightly larger than the closed packed periodicity of ChHP small molecules in crystalline form of 4.7 nm as determined by SAXS (S3.1) and can be assigned to the periodicity of P4VP(ChHP) comb block. Upon heating to 120 °C, the first-order peak originated from small molecule shifts to a lower q value while its second-order peak disappears, suggesting that the ChHP molecules are no longer assembled into ordered layers inside the P4VP(ChHP) microdomain. At 130 °C, the ChHP peaks completely disappear, and the periodicity of the BCP supramolecule decreases further to 28.2 nm (q = 0.223 Å^{-1}). There is a gradual decrease in the BCP periodicity with further increase in temperature. At 150 °C the SAXS profile indicates a BCP periodicity of 27.2 nm.

dx.doi.org/10.1021/ma401033w | *Macromolecules* 2013, 46, 5531−5537

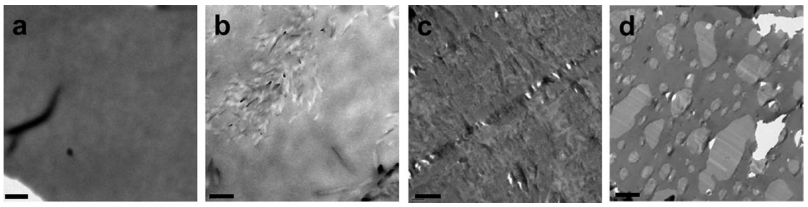

Figure 3. Low-magnification TEM images of a PS(24k)-*b*-P4VP(9.5k)$_1$(ChHP)$_1$ (a) as cast, (b) annealed at 110 °C for 12 h, (c) annealed at 130 °C for 12 h, and (d) annealed at 150 °C for 12 h. The appearance of phase-separated ChHP is observed in samples annealed at temperatures higher than 110 °C as brighter regions. Scale bars are 1 μm for all images.

Upon cooling the supramolecule from 150 °C to room temperature, the BCP periodicity only increases slightly. At 110 °C, a peak at q = 0.14 Å^{-1} appears, similar to that of the crystallized ChHP. The same family of supramolecules with different compositions was also studied. Similar trends of decrease in BCP periodicity during heating and appearance of the ChHP crystallization peak during cooling are observed (Figure 1, middle and right panels). For the PS(40k)-*b*-P4VP(5.6k)$_1$(ChHP)$_1$ supramolecule (Figure 1, right panel), scattering peaks indicating a lamellar BCP morphology (1:2:3:4) are clearly visible at 110 °C. As the temperature increases to 140 °C, the scattering peak ratios change to $1:\sqrt{3}:\sqrt{4}$, a clear indication of a transition between lamellar and hexagonally packed cylinder morphology.

The *in situ* SAXS studies suggest that the supramolecule undergoes thermoresponsive, nonreversible changes such as decrease in periodicity of BCP and ChHP packing. These drastic changes lead to a range of morphological transitions, such as cylinder-to-lamellae and lamellae-to-inverse cylinder, in the supramolecule.

Transmission electron microscopy (TEM) was used to characterize the morphology of the supramolecules. For the PS(24k)-*b*-P4VP(9.5k)$_1$(ChHP)$_1$ (Figure 2a), the unannealed sample forms a morphology with hexagonally packed PS cylinders embedded in the P4VP(ChHP) matrix, consistent with the volume fraction of the P4VP(ChHP) block, $f_{P4VP(ChHP)}$ = 0.721. After being annealed at 130 °C, there is a clear morphological transition from cylinder to lamellar. When the annealing temperature is increased further to 150 °C, inverse cylinder was seen, in which the majority block is now the unstained polystyrene block, appearing as the lighter phase.

TEM studies were carried out for the two other supramolecules, PS(19k)-*b*-P4VP(5.2k)$_1$(ChHP)$_1$ ($f_{P4VP(ChHP)}$ = 0.641) (Figure 2b) and PS(40k)-*b*-P4VP(5.6k)$_1$(ChHP)$_1$ ($f_{P4VP(ChHP)}$ = 0.477) (Figure 2c), to determine whether such temperature driven OOTs are common for this supramolecular system. For the PS(19k)-*b*-P4VP(5.2k)$_1$(ChHP)$_1$, TEM (Figure 2b) shows that the unannealed sample has a mixture of P4VP(ChHP) majority cylindrical morphology and lamellar morphology. This is consistent with the comb block volume fraction for this supramolecule, which lies at the boundary of lamellar and cylindrical morphology. At higher annealing temperatures, the morphology transitions to a lamellar morphology at 130 °C and then an inverse cylindrical morphology at 150 °C. Similar thermally induced morphological transitions were observed for the PS(40k)-*b*-P4VP(5.6k)$_1$(ChHP)$_1$, i.e., from lamellar (<130 °C) to inverse cylindrical microdomains (150 °C) (Figure 2c). TEM suggests that the morphological transitions during thermal annealing represent a general phenomenon for this supramolecular system. The final morphologies are further corroborated with SAXS of the supramolecule samples after thermal annealing (Figure S2). The morphologies after cooling are stable at room temperature and precisely tunable by annealing temperature.

The macrophase separation of the ChHP molecules is visible from TEM images taken at lower magnification (Figure 3). For all three supramolecules, the unannealed sample has a uniform composition. At higher annealing temperatures, a second brighter phase begins to appear, and the sizes of the second phase increase as the annealing temperature increases. A zoomed-in view of the interface between the bright and dark phases show that the dark phase is the microphase-separated PS-*b*-P4VP(ChHP) supramolecule, while the bright phase should be ChHP-rich. The interface between PS-*b*-P4VP-(ChHP) and macrophase-separated ChHP is very sharply defined, and both PS and P4VP(ChHP) microdomains reside at the interface (Figure 4). This suggests that the "free" ChHP

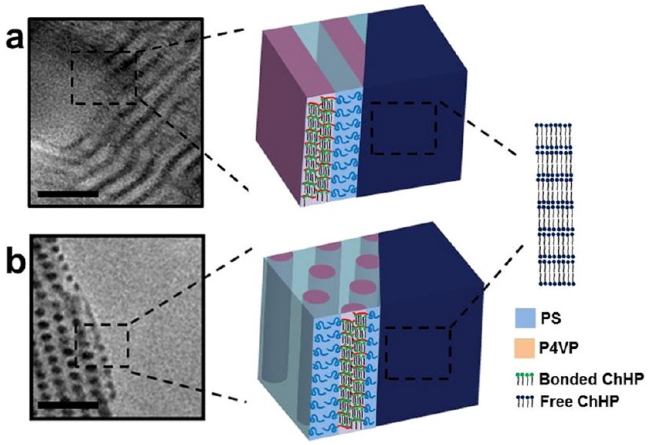

Figure 4. TEM images (left) showing the sharp interface between the (a) lamellar and (b) cylindrical microdomains in PS-*b*-P4VP(ChHP) phase and the crystalline ChHP phase. The schematic (right) shows a structural view of the interface. Scale bars are 100 nm.

molecules that have diffused out of the P4VP microdomain during thermal annealing do not diffuse back to either the PS or P4VP(ChHP) microdomains, and the free ChHP forms into a macrophase-separated crystalline phase.

These observations, coupled with the *in situ* SAXS and TEM data, provide a more detailed picture for the observed morphological transitions in this supramolecular system (Figure 5). At room temperature, the solvent-cast supramolecule adopts a morphology that is expected from the calculated volume fraction of the supramolecule assuming complete incorporation of ChHP into the P4VP microdomain. Upon heating of the supramolecule, several morphological transitions take place on the length scales of both the BCP and ChHP. The comb structure of P4VP(ChHP) disintegrates above 120 °C as ChHP

dx.doi.org/10.1021/ma401033w | *Macromolecules* 2013, 46, 5531−5537

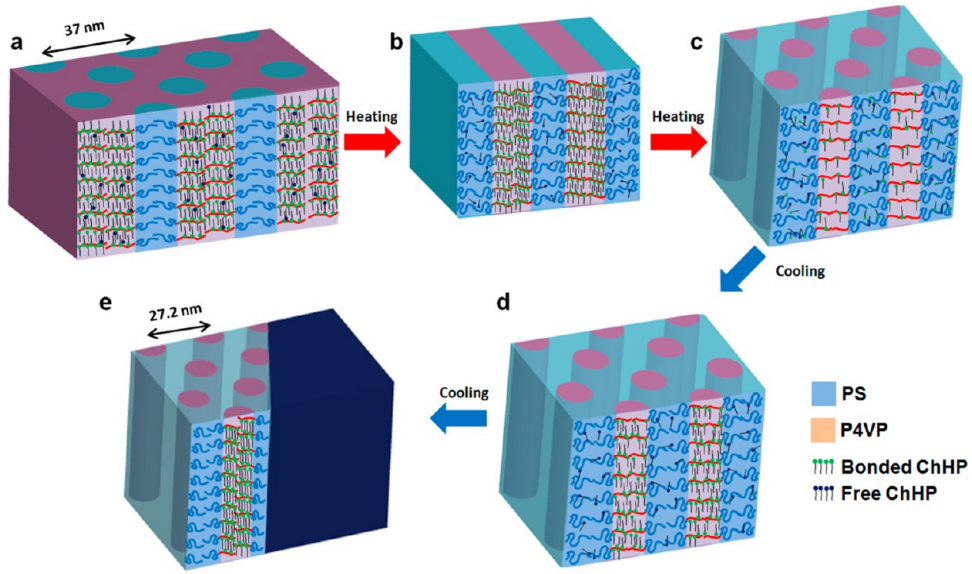

Figure 5. Schematic showing the mechanism of the observed phase transitions of PS-*b*-P4VP(ChHP) during heating and cooling (specifically pertaining to inverse cylinder−lamellar cylinder transitions observed in PS(24k)-*b*-P4VP(9.5k)$_1$(ChHP)$_1$). (a) Below 120 °C, all ChHP molecules are confined in P4VP microdomain. (b) As temperature reaches 120 °C, unbonded ChHP molecules start to diffuse out of P4VP microdomain. (c) Further diffusion of ChHP molecules out of P4VP microdomain causes OOTs to P4VP(ChHP) minority phase. (d) Cooling below 130 °C causes some ChHP to re-form hydrogen bond with P4VP. (e) Further cooling below T_m of ChHP causes crystallization of unbounded ChHP in a separate phase.

molecules diffuse out of the P4VP microdomain and the supramolecule periodicity decreases (Figure 5b). The overall supramolecular morphology undergoes two OOTs spanning a wide range of $f_{P4VP(ChHP)}$, from P4VP(ChHP)-majority cylinders to P4VP(ChHP)-minority inverse cylinders (Figure 5c). Upon cooling below 130 °C, only a small fraction of ChHP molecules diffuse back into the P4VP microdomain (Figure 5d), while the remaining ChHP molecules crystallize in separate, sharply defined macrophase that help preserve the high-temperature supramolecule morphologies (Figure 5e). The sharp interface between the two macrophases further ensures the uniformity of obtained nanostructures.

There are several possible mechanisms to explain the observed nonreversible OOTs. The hydrogen bonding between 4VP and ChHP is the main driving force to sequester ChHP within P4VP(ChHP) microdomains. Upon heating, the H-bonds start to break. *In situ* FTIR measurements were carried out using a P4VP(46.7k)$_1$(ChHP)$_1$ supramolecule during heating from room temperature to 150 °C (Figure 6). At room temperature, the FTIR spectrum of the supramolecule has absorption peaks at 1011 and 1602 cm^{-1}, characteristic of a stretched pyridine ring and indicating the formation of hydrogen bonds between 4VP and ChHP. As the temperature increases, the intensity of the 1011 cm^{-1} peak decreases slightly, accompanied by the appearance of a peak at 993 cm^{-1} around 120 °C, corresponding to free 4VP.[27,28,34,35] In addition, the 1602 cm^{-1} peak shifts to 1597 cm^{-1}. This indicates the destabilization of the phenol−pyridine hydrogen bonding at T > 120 °C. Upon cooling, the 993 cm^{-1} peak disappears and the 1011 cm^{-1} peak reappears, while the 1597 cm^{-1} peak shifts back to 1602 cm^{-1}, suggesting that the hydrogen-bonded complex between P4VP and ChHP is thermally reversible, similar to that seen in the supramolecular systems based on alkylphenol.[28] Thus, hydrogen bond breaking cannot be the sole explanation for nonreversible OOTs observed in this supramolecular system.

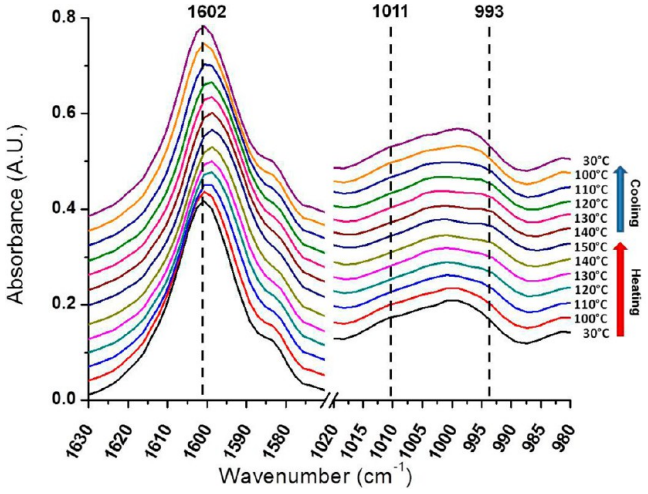

Figure 6. *In situ* FTIR spectra of P4VP(46.7k)$_1$(ChHP)$_1$ heated from 30 °C (bottom) to 150 °C and subsequently cooled back to 30 °C (top). Absorption peaks corresponding to unstretched 4VP units (993 and 1597 cm^{-1}) appear above 120 °C during both heating and cooling cycles, signifying destabilization of hydrogen bonding at higher temperatures.

A change in χ is known to induce OOTs in BCP systems because the phase boundaries in a BCP system are curved with respect to χ and volume fraction f of each block.[36] It is reasonable to believe the Flory−Huggins interaction parameter χ between the PS and P4VP(ChHP) blocks decreases with increasing temperature. However, such morphological transitions were typically observed over a narrow range of volume fraction of one component and are typically thermally reversible. Therefore, this cannot explain the nonreversible OOTs that occur over a wide range of volume fractions observed here.

dx.doi.org/10.1021/ma401033w | *Macromolecules* 2013, 46, 5531−5537

Rather, the observed OOTs may be due to a combination of three factors, i.e., increased miscibility between PS and ChHP at high temperatures, slow diffusion of ChHP back into the P4VP(ChHP) microdomain during cooling due to steric repulsion between ChHP small molecules, and reduced mobility of ChHP due to crystallization upon cooling. The increased PS/ChHP miscibility at high temperatures would result in the diffusion of ChHP from the P4VP to the PS microdomain during thermal annealing, thereby resulting in a significant decrease in $f_{P4VP(ChHP)}$ and inducing OOTs over a wide morphology range. This is similar to the mechanism proposed by Ikkala et al. in their investigation of the supramolecule comprising of PS-*b*-P4VP and 3-pentadecylphenol (PDP).[28] The miscibility of ChHP in PS is evident from differential scanning calorimetry (DSC), showing a depression in the T_g of PS from 104 to 91 °C (S3.3). The extent of PS/ChHP miscibility is further confirmed via polarized optical microscopy (POM) studies (S3.4). PS and ChHP have low miscibility (~10 wt % ChHP in PS) at room temperature. At higher ChHP loadings (30−50 wt %), ChHP molecules crystallize to form a separate birefringent macrophase. As the temperature increases to above 135 °C, the birefrigent crystalline phase disappears instantaneously, suggesting high solubility of ChHP in PS. Upon cooling of the mixture to below 135 °C, the birefringent phase reappears, suggesting that ChHP crystallizes. From these observations, it is evident that at high annealing temperatures there is a strong driving force for ChHP to diffuse into the PS microdomain. This phase behavior is in contrast with the supramolecular system based on oligothiophene (4T), PS-*b*-P4VP(4T) system reported by Rancatore et al.[30] 4T has an even higher crystallization temperature than ChHP but has a linear molecular shape that is more conducive to close packing, so that crystallization occurs within the P4VP microdomain rather than within a separate macrophase. In addition, another key difference between the PS-*b*-P4VP(ChHP) system and the PS-*b*-P4VP(PDP) system is that upon cooling the PDP becomes immiscible with the PS microdomain and the small molecules reincorporate into the P4VP microdomain, resulting in a thermoreversibility in the OOTs. For the PS-*b*-P4VP(ChHP) supramolecule, however, during cooling there is a competition between diffusion of ChHP back into the P4VP microdomain and crystallization of ChHP into a separate macrophase. Clearly, crystallization of ChHP dominates, although a small fraction of ChHP does diffuse back into the P4VP microdomain, resulting in the re-formation of some 4VP/ChHP hydrogen bonds.

The dominance of ChHP crystallization over reversible diffusion is possibly due to two factors. One is that ChHP has a higher crystallization temperature (~135 °C) than PDP (~55 °C),[28,35] such that upon cooling ChHP crystallizes while still being highly miscible within PS. On the other hand, we hypothesize that PDP's crystallization temperature may be below the PDP/PS miscibility gap (Figure 7); thus, PDP small molecules tend to diffuse back into the P4VP microdomain upon cooling. We hypothesize that there are additional driving forces, specific to the ChHP molecule, that prevent the reincorporation of ChHP into the P4VP microdomain. The ChHP molecule contains a bulky cholesteric group, which may affect its molecular packing and introduces intermolecular steric repulsion that may further slow the diffusion of ChHP back into the P4VP microdomain. This slowed diffusion can be seen in PS-*b*-P4VP(ChHP) samples that are cooled on a longer time scale, with temperatures decreasing from 150 to 100 °C over 4 h (Supporting Information S4). The resulting morphologies are similar to the samples cooled within 1 h, suggesting no significant changes in the diffusion of ChHP back into P4VP due to the slower cooling rate.

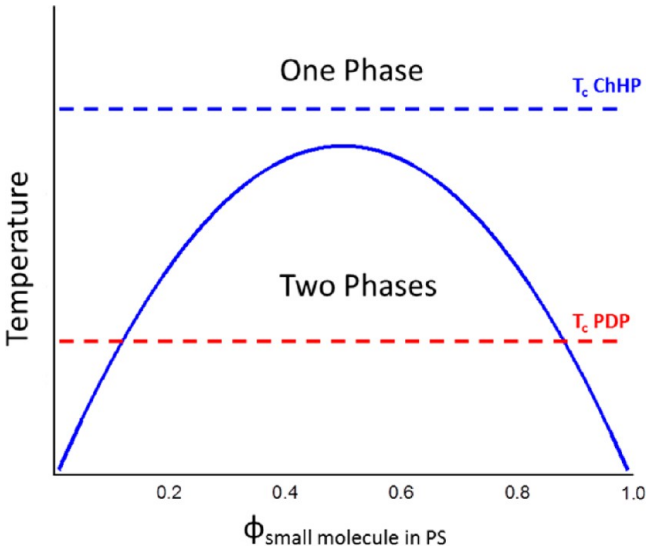

Figure 7. Hypothetical plot demonstrating the crystallization temperature of ChHP and PDP relative to the miscibility in PS microdomain.

CONCLUSION

In this study, we investigated the thermoresponsive phase behavior of a block copolymer-based supramolecule containing a liquid crystal small molecule, PS-*b*-P4VP(ChHP), using DSC, POM, TEM, SAXS, and FTIR. Upon thermal annealing, the supramolecule underwent a series of nonreversible OOTs from a P4VP(ChHP) block majority phase to a P4VP(ChHP) block minority phase, which is explained by the diffusion of ChHP out of the P4VP(ChHP) block during heating, and subsequent crystallization of free ChHP into a separate phase during cooling due to the high T_m of ChHP and the steric repulsion between bonded and free ChHP. The OOTs are nonreversible upon cooling; therefore, the morphologies generated during thermal annealing are stable at room temperature and tunable by adjusting the thermal annealing temperature. This study highlights the important role of small molecule phase behavior, miscibility, and intermolecular interactions on the overall thermal phase behavior of BCP-based supramolecules containing these small molecules. In addition, this supramolecular system provides a robust platform to generate multiple morphologies from a single starting material.

ASSOCIATED CONTENT

Supporting Information

Experimental details for the preparation and characterization of ChHP small molecule; TEM of PS-*b*-P4VP(ChHP) supramolecule thermally annealed and cooled at slower rate. This material is available free of charge via the Internet at http://pubs.acs.org.

AUTHOR INFORMATION

Corresponding Author

*E-mail: tingxu@berkeley.edu (T.X.).

Present Address

[‖]M.I.K.: Samsung Display, 95, Samsung 2-ro, Giheung-gu, Yongin-si, Gyeonggi-do, Korea.

Notes

The authors declare no competing financial interest.

■ ACKNOWLEDGMENTS

We thank Dr. Clayton Mauldin and Prof. Jean Fréchet for providing ChHP for initial studies. This work was supported by the National Science Foundation under Contract DMR-1007002. The Advanced Light Source is supported by the Director, Office of Science, Office of Basic Energy Sciences, of the U.S. Department of Energy under Contract DE-AC02-05CH11231.

■ REFERENCES

(1) Valkama, S.; Ruotsalainen, T.; Nykanen, A.; Laiho, A.; Kosonen, H.; ten Brinke, G.; Ikkala, O.; Ruokolainen, J. *Macromolecules* **2006**, *39* (26), 9327−9336.
(2) Kato, T.; Frechet, J. M. J. *Macromolecules* **1989**, *22* (9), 3818−3819.
(3) Ikkala, O.; ten Brinke, G. *Chem. Commun.* **2004**, *19*, 2131−2137.
(4) Wurthner, F.; Chen, Z. J.; Hoeben, F. J. M.; Osswald, P.; You, C. C.; Jonkheijm, P.; von Herrikhuyzen, J.; Schenning, A.; van der Schoot, P.; Meijer, E. W.; Beckers, E. H. A.; Meskers, S. C. J.; Janssen, R. A. J. *J. Am. Chem. Soc.* **2004**, *126* (34), 10611−10618.
(5) Tang, C.; Lennon, E. M.; Fredrickson, G. H.; Kramer, E. J.; Hawker, C. J. *Science* **2008**, *322* (5900), 429−432.
(6) Antonietti, M.; Conrad, J. *Angew. Chem., Int. Ed. Engl.* **1994**, *33* (18), 1869−1870.
(7) Fyfe, M. C. T.; Stoddart, J. F. *Acc. Chem. Res.* **1997**, *30* (10), 393−401.
(8) Stewart, D.; Imrie, C. T. *Macromolecules* **1997**, *30* (4), 877−884.
(9) Soininen, A. J.; Tanionou, I.; ten Brummelhuis, N.; Schlaad, H.; Hadjichristidis, N.; Ikkala, O.; Raula, J.; Mezzenga, R.; Ruokolainen, J. *Macromolecules* **2012**, *45* (17), 7091−7097.
(10) Faul, C. F. J.; Antonietti, M. *Adv. Mater.* **2003**, *15* (9), 673−683.
(11) Schubert, U. S.; Eschbaumer, C. *Angew. Chem., Int. Ed.* **2002**, *41* (16), 2893−2926.
(12) Hoeben, F. J. M.; Jonkheijm, P.; Meijer, E. W.; Schenning, A. *Chem. Rev.* **2005**, *105* (4), 1491−1546.
(13) Pollino, J. M.; Weck, M. *Chem. Soc. Rev.* **2005**, *34* (3), 193−207.
(14) Chao, C. Y.; Li, X. F.; Ober, C. K.; Osuji, C.; Thomas, E. L. *Adv. Funct. Mater.* **2004**, *14* (4), 364−370.
(15) Gopinadhan, M.; Majewski, P. W.; Beach, E. S.; Osuji, C. O. *ACS Macro Lett.* **2012**, *1* (1), 184−189.
(16) del Barrio, J.; Blasco, E.; Oriol, L.; Alcala, R.; Sanchez-Somolinos, C. *J. Polym. Sci., Part A: Polym. Chem.* **2013**, *51* (8), 1716−1725.
(17) Sary, N.; Richard, F.; Brochon, C.; Leclerc, N.; Leveque, P.; Audinot, J.-N.; Berson, S.; Heiser, T.; Hadziioannou, G.; Mezzenga, R. *Adv. Mater.* **2010**, *22* (6), 763.
(18) Yao, K.; Chen, L.; Li, F.; Wang, P.; Chen, Y. *J. Phys. Chem. C* **2012**, *116* (1), 714−721.
(19) Majewski, P. W.; Gopinadhan, M.; Jang, W.-S.; Lutkenhaus, J. L.; Osuji, C. O. *J. Am. Chem. Soc.* **2010**, *132* (49), 17516−17522.
(20) Majewski, P. W.; Gopinadhan, M.; Osuji, C. O. *J. Polym. Sci., Part B: Polym. Phys.* **2012**, *50* (1), 2−8.
(21) Zhao, Y.; Thorkelsson, K.; Mastroianni, A. J.; Schilling, T.; Luther, J. M.; Rancatore, B. J.; Matsunaga, K.; Jinnai, H.; Wu, Y.; Poulsen, D.; Frechet, J. M. J.; Alivisatos, A. P.; Xu, T. *Nat. Mater.* **2009**, *8* (12), 979−985.
(22) Ruokolainen, J.; Torkkeli, M.; Serimaa, R.; Vahvaselka, S.; Saariaho, M.; tenBrinke, G.; Ikkala, O. *Macromolecules* **1996**, *29* (20), 6621−6628.
(23) Ruokolainen, J.; ten Brinke, G.; Ikkala, O.; Torkkeli, M.; Serimaa, R. *Macromolecules* **1996**, *29* (10), 3409−3415.
(24) Bazuin, C. G.; Brandys, F. A. *Chem. Mater.* **1992**, *4* (5), 970−972.
(25) Talroze, R. V.; Kuptsov, S. A.; Sycheva, T. I.; Bezborodov, V. S.; Plate, N. A. *Macromolecules* **1995**, *28* (25), 8689−8691.
(26) Valkama, S.; Kosonen, H.; Ruokolainen, J.; Haatainen, T.; Torkkeli, M.; Serimaa, R.; Ten Brinke, G.; Ikkala, O. *Nat. Mater.* **2004**, *3* (12), 872−876.
(27) Korhonen, J. T.; Verho, T.; Rannou, P.; Ikkala, O. *Macromolecules* **2010**, *43* (3), 1507−1514.
(28) Ruokolainen, J.; Makinen, R.; Torkkeli, M.; Makela, T.; Serimaa, R.; ten Brinke, G.; Ikkala, O. *Science* **1998**, *280* (5363), 557−560.
(29) Rancatore, B. J.; Mauldin, C. E.; Tung, S. H.; Wang, C.; Hexemer, A.; Strzalka, J.; Fréchet, J. M. J.; Xu, T. *ACS Nano* **2010**, *4* (5), 2721−2729.
(30) Rancatore, B. J.; Mauldin, C. E.; Frechet, J. M. J.; Xu, T. *Macromolecules* **2012**, *45* (20), 8292−8299.
(31) Hammond, M. R.; Mezzenga, R. *Soft Matter* **2008**, *4* (5), 952−961.
(32) de Wit, J.; van Ekenstein, G. A.; Polushkin, E.; Kvashnina, K.; Bras, W.; Ikkala, O.; ten Brinke, G. *Macromolecules* **2008**, *41* (12), 4200−4204.
(33) Tung, S.-H.; Xu, T. *Macromolecules* **2009**, *42* (15), 5761−5765.
(34) Ruokolainen, J.; Saariaho, M.; Ikkala, O.; ten Brinke, G.; Thomas, E. L.; Torkkeli, M.; Serimaa, R. *Macromolecules* **1999**, *32* (4), 1152−1158.
(35) Ruokolainen, J.; ten Brinke, G.; Ikkala, O. *Adv. Mater.* **1999**, *11* (9), 777−780.
(36) Khandpur, A. K.; Forster, S.; Bates, F. S.; Hamley, I. W.; Ryan, A. J.; Bras, W.; Almdal, K.; Mortensen, K. *Macromolecules* **1995**, *28* (26), 8796−8806.